Mobile Target Tracking Using an Unmanned Aerial Vehicle with a Non-Gimbaled Video Sensor

Conference Paper · January 2015

DOI: 10.2514/6.2015-1077

2 authors:

Liang Sun
New Mexico State University
46 PUBLICATIONS **219** CITATIONS
SEE PROFILE

D. Pack
University of Texas at San Antonio
88 PUBLICATIONS **760** CITATIONS
SEE PROFILE

AIAA SciTech
5-9 January 2015, Kissimmee, Florida
AIAA Guidance, Navigation, and Control Conference

Mobile Target Tracking Using an Unmanned Aerial Vehicle with a Non-Gimbaled Video Sensor

Liang Sun * and Daniel Pack †

In this paper, we present a novel path planning strategy for an unmanned aerial vehicle (UAV) with a non-gimbaled video sensor to track a ground mobile target. A 3-dimensional UAV dynamic model is used in the proposed optimization strategy to incorporate the coupled relationship between the camera line-of-sight and UAV motion. Two mathematical formulations are proposed to derive the objective function used in a Model Predictive Control (MPC) technique. We also develop a dynamic window based technique to take agile target motion into account when determining the receding horizon time period used in the MPC. In addition, the influence of different sensor placements and time horizons toward generating desired UAV trajectories are studied. Simulation results are presented to show the effectiveness of the proposed approach in tracking a target moving with different trajectory patterns.

I. Introduction

In mobile target tracking missions executed by Unmanned Aerial Vehicles (UAVs), gimbaled sensors are typically used to track targets, provided that the target moves slower than the UAV. However, the extra payload to support a robust gimbaled sensor is an expensive cost for small UAVs against flight duration. On the other hand, the hardware simplicity of using a fixed image sensor introduces new challenges for an onboard controller to incorporate real-time sensor needs to UAV's dynamic trajectory planning. With a fixed sensor, a UAV is more likely to fail to 'see' a target, requiring sophisticated estimation and motion prediction techniques. In addition, it is not practical to use traditional optimization methods since the dynamic nature of target is typically unknown to the UAV, forcing the need to develop a new type of real-time optimization method.

Some related efforts have been reported in the literature. Dobrokhodov et al.[1] proposed a 2-D guidance law for a UAV with a gimbaled camera to track a mobile ground target. A nonlinear filter was used to produce estimates of target location and velocity. Flight test results showed the superior performance of the estimator when compared to the ones from their previous work[2] and one resulted from using a parameter varying technique.[3] Geiger et al.[4] presented an optimal strategy to maximize the time of target observation. In this work, the location of a ground target was projected onto the camera plane to minimize the distance of the projected point from the center of the image plane. The target location was assumed, however, to be always available and no estimation was used to evaluate the system performance. Geiger et al.[4–6] also reported a target tracking algorithm using a single camera which points downwards at all times. Focusing on the path planning portion of the task, Amin et al.[7] utilized a modified Rapidly-exploring Random Tree method and the Dijkstra's algorithm to find a sub-optimal path of a moving platform. Toupet and Mettler[8] developed a path planner for an unmanned helicopter using a combination of mixed integer linear programming to generate a local path and a near real-time dynamic programming for a global path using the cost-to-go map. Rysdyk[9] derived a UAV control law to track a moving target with a gimbaled camera in Serret-Frenet coordinates. Simulation results showed the impact of wind on the stabilized camera angles and the proposed algorithm was able to maintain a constant line of sight to the target in the aircraft body frame in the presence of mild winds.

In this paper, we describe an overall approach of solving a target tracking and engagement problem using a non-gimbaled sensor on a high speed autonomous aerial vehicle. The main contributions include two mathematical formulations for the motion interplay between an aerial vehicle and a surface/ground target using a non-gimbaled image sensor, impact of sensor placement to resulting UAV trajectories, and an optimal path planning technique using a dynamic time horizon window.

*Postdoc Research Fellow, Department of Electrical and Computer Engineering, The University of Texas at San Antonio, Texas, USA. liang.sun@utsa.edu

†Professor, Department of Electrical and Computer Engineering, The University of Texas at San Antonio, Texas, USA. daniel.pack@utsa.edu

The rest of the paper is structured as follows. Section II presents a UAV dynamic model used. Two mathematical formulations for the cost function used in an optimal path planning technique are introduced in Section III. In Section IV, we present the influence of different sensor configurations to desired UAV trajectories for tracking a particular target motion. A dynamic time horizon window based optimization technique is proposed in Section V. Preliminary results are presented in Section VII, and Section VIII concludes the paper.

II. Platform Dynamics

In a typical target tracking mission using a UAV with a gimbaled sensor, UAV dynamics are analyzed in a 2-D plane, i.e., the altitude of the platform is constant, which would not be a valid assumption for a UAV with a non-gimbaled camera. In this paper, the following 3-D UAV motion model is used.[10]

$$\begin{pmatrix} \dot{p}_{u_n} \\ \dot{p}_{u_e} \\ \dot{p}_{u_d} \end{pmatrix} = \begin{pmatrix} \mathrm{c}_\theta \mathrm{c}_\psi & \mathrm{s}_\phi \mathrm{s}_\theta \mathrm{c}_\psi - \mathrm{c}_\phi \mathrm{s}_\psi & \mathrm{c}_\phi \mathrm{s}_\theta \mathrm{c}_\psi + \mathrm{s}_\phi \mathrm{s}_\psi \\ \mathrm{c}_\theta \mathrm{s}_\psi & \mathrm{s}_\phi \mathrm{s}_\theta \mathrm{s}_\psi + \mathrm{c}_\phi \mathrm{c}_\psi & \mathrm{c}_\phi \mathrm{s}_\theta \mathrm{s}_\psi - \mathrm{s}_\phi \mathrm{c}_\psi \\ -\mathrm{s}_\theta & \mathrm{s}_\phi \mathrm{c}_\theta & \mathrm{c}_\phi \mathrm{c}_\theta \end{pmatrix} \begin{pmatrix} u \\ v \\ w \end{pmatrix}, \tag{1}$$

where c_x and s_x denote $\cos x$ and $\sin x$, respectively, $\mathbf{p}_u \triangleq (p_{u_n}, p_{u_e}, p_{u_d})^T \in \mathbb{R}^3$ is defined as the UAV position in the North-East-Down (NED) inertial frame, (u, v, w) is the body-frame velocity vector, and ϕ, θ and ψ are the roll, pitch and yaw angles, respectively. The UAV body-frame acceleration can be calculated as

$$\begin{pmatrix} \dot{u} \\ \dot{v} \\ \dot{w} \end{pmatrix} = \begin{pmatrix} rv - qw \\ pw - ru \\ qu - pv \end{pmatrix} + \frac{1}{m} \begin{pmatrix} f_x \\ f_y \\ f_z \end{pmatrix}, \tag{2}$$

where m is the vehicle mass, (p, q, r) is the rotational velocity of (ϕ, θ, ψ) measured in the body frame, and (f_x, f_y, f_z) is the sum of externally applied forces defined in the body frame. The rotational velocity and acceleration of the vehicle frame with respect to the body frame are modeled as

$$\begin{pmatrix} \dot{\phi} \\ \dot{\theta} \\ \dot{\psi} \end{pmatrix} = \begin{pmatrix} 1 & \sin\phi \tan\theta & \cos\phi \tan\theta \\ 0 & \cos\phi & -\sin\phi \\ 0 & \frac{\sin\phi}{\cos\theta} & \frac{\cos\phi}{\cos\theta} \end{pmatrix} \begin{pmatrix} p \\ q \\ r \end{pmatrix}, \tag{3}$$

$$\begin{pmatrix} \dot{p} \\ \dot{q} \\ \dot{r} \end{pmatrix} = \begin{pmatrix} \Gamma_1 pq - \Gamma_2 qr \\ \Gamma_5 pr - \Gamma_6 \left(p^2 - r^2\right) \\ \Gamma_7 pq - \Gamma_1 qr \end{pmatrix} + \begin{pmatrix} \Gamma_3 u_l + \Gamma_4 u_n \\ \frac{1}{J_y} u_m \\ \Gamma_4 u_l + \Gamma_8 u_n \end{pmatrix}. \tag{4}$$

where parameters Γ_* are given by

$$\begin{aligned} \Gamma_1 &= \frac{J_{xz}\left(J_x - J_y + J_z\right)}{\Gamma} \\ \Gamma 2 &= \frac{J_z\left(J_z - J_y\right) + J_{xz}^2}{\Gamma} \\ \Gamma_3 &= \frac{J_z}{\Gamma} \\ \Gamma 4 &= \frac{J_{xz}}{\Gamma} \\ \Gamma_5 &= \frac{J_z - J_x}{J_y} \\ \Gamma_6 &= \frac{J_{xz}}{J_y} \\ \Gamma_7 &= \frac{\left(J_x - J_y\right) J_x + J_{xz}^2}{\Gamma} \\ \Gamma_8 &= \frac{J_x}{\Gamma}, \\ \Gamma &= J_x J_z - J_{xz}^2 \end{aligned}$$

where J_x, J_y and J_z are moments of inertia of the UAV and (u_l, u_m, u_n) is the sum of externally applied moments about the UAV body frame.

III. Optimal Path Planning

The objective of the path planning algorithm is to find control inputs (f_x, f_y, f_z) and (u_l, u_m, u_n) in Equations 2 and 4, respectively, such that the resulting motion of the UAV with a non-gimbaled camera will maximize target observation time for a varying time window T_s. We first define binary variable s as

$$s \triangleq \begin{cases} 1 & \text{Target seen by camera,} \\ 0 & \text{No target seen by camera.} \end{cases} \tag{5}$$

Then, the problem of maximizing target observation time becomes one that maximizes the following cost function

$$\Sigma = \int_0^{T_s} s\left(\tau\right) \Phi \mathrm{d}\tau, \tag{6}$$

where Φ represents two different functions we will describe in the following subsections to maximize the target observation time.

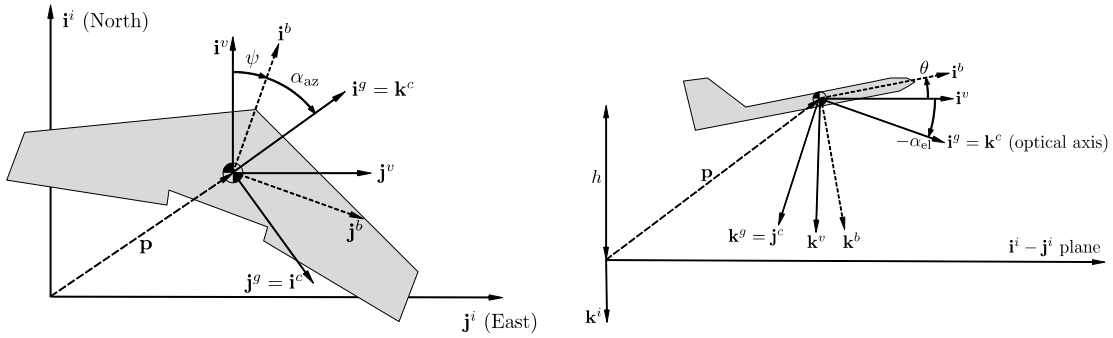

(a) Top-down view of coordinate frames.

(b) Side view of coordinate frames.

Figure 1. Coordinate frames: Inertial frame: $\mathcal{F}^i = (\mathbf{i}^i, \mathbf{j}^i, \mathbf{k}^i)$, **Vehicle frame:** $\mathcal{F}^v = (\mathbf{i}^v, \mathbf{j}^v, \mathbf{k}^v)$, **Body frame:** $\mathcal{F}^b = (\mathbf{i}^b, \mathbf{j}^b, \mathbf{k}^b)$, **Gimbal frame:** $\mathcal{F}^g = (\mathbf{i}^g, \mathbf{j}^g, \mathbf{k}^g)$, **and Camera frame:** $\mathcal{F}^c = (\mathbf{i}^c, \mathbf{j}^c, \mathbf{k}^c)$.[10]

To proceed forward, the coordinate frames shown in Figure 1 are used to derive rotation matrices R_b^v, R_g^b and R_c^g, which transform a vector from the body frame to the vehicle frame, from the gimbal frame to the body frame, and from the camera frame to the gimbal frame, respectively. The rotation matrices are given as

$$R_b^v \triangleq \begin{pmatrix} \mathrm{c}_\theta \mathrm{c}_\psi & \mathrm{s}_\phi \mathrm{s}_\theta \mathrm{c}_\psi - \mathrm{c}_\phi \mathrm{s}_\psi & \mathrm{c}_\phi \mathrm{s}_\theta \mathrm{c}_\psi + \mathrm{s}_\phi \mathrm{s}_\psi \\ \mathrm{c}_\theta \mathrm{s}_\psi & \mathrm{s}_\phi \mathrm{s}_\theta \mathrm{s}_\psi + \mathrm{c}_\phi \mathrm{c}_\psi & \mathrm{c}_\phi \mathrm{s}_\theta \mathrm{s}_\psi - \mathrm{s}_\phi \mathrm{c}_\psi \\ -\mathrm{s}_\theta & \mathrm{s}_\phi \mathrm{c}_\theta & \mathrm{c}_\phi \mathrm{c}_\theta \end{pmatrix}, \tag{7}$$

$$R_g^b \triangleq \begin{pmatrix} \cos\alpha_{el} \cos\alpha_{az} & \cos\alpha_{el} \sin\alpha_{az} & -\sin\alpha_{el} \\ -\sin\alpha_{az} & \cos\alpha_{az} & 0 \\ \sin\alpha_{el} \cos\alpha_{az} & \sin\alpha_{el} \sin az & \cos\alpha_{el} \end{pmatrix}, \tag{8}$$

$$R_c^g \triangleq \begin{pmatrix} 0 & 0 & 1 \\ 1 & 0 & 0 \\ 0 & 1 & 0 \end{pmatrix}, \tag{9}$$

where α_{el} and α_{az} are elevation and azimuth angles of the gimbal. For the current application of non-gimbaled camera, both R_g^b and R_c^g are constant matrices, reflecting fixed coordinate relationships.

We define positive variable ξ, shown in Figure 2, as the angle between the optical axis of the gimbal, $\mathbf{i}^g$, and the unit vector that connects a target to the UAV, which is defined by

$$\mathbf{n}_{ut}^v \triangleq \frac{\mathbf{p}_t - \mathbf{p}_u}{\|\mathbf{p}_t - \mathbf{p}_u\|}, \tag{10}$$

where $\mathbf{p}_t = (p_{t_n}, p_{t_e}, p_{t_d})^T$ is the target position in the inertial frame. With the camera field of view defined as μ, we have

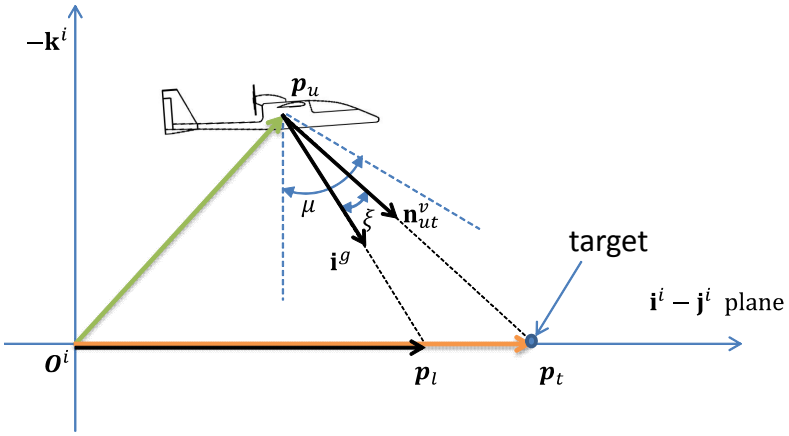

Figure 2. Relationship between a camera's optical axis and the vector connecting UAV and a target (Method 1) and distance between the target location and the intersection of the camera optical axis and the ground plane (Method 2).

$$s = \begin{cases} 1 & \xi \leq \frac{\mu}{2}, \\ 0 & \xi > \frac{\mu}{2}, \end{cases} \tag{11}$$

which is equivalent to

$$s = \frac{1}{2}\left(1 + \operatorname{sgn}\left(\xi - \frac{\mu}{2}\right)\right), \tag{12}$$

where

$$\operatorname{sgn}(x) = \begin{cases} 1 & x \leq 0, \\ 0 & x > 0. \end{cases}$$

Then, Equation (6) becomes

$$\Sigma = \int_0^{T_s} \frac{1}{2}\left(1 + \operatorname{sgn}\left(\xi - \frac{\mu}{2}\right)\right) \Phi \mathrm{d}\tau, \tag{13}$$

In the subsequent subsections, we present two different formulation of Φ.

A. Method 1

The method proposed in this subsection aims to minimize the angle between the optical axis and the vector connecting the UAV to the target. We first define a unit vector that represents the direction of the camera optical axis, $\mathbf{n}_{axis}$, in the gimbal frame as $\mathbf{n}_{axis}^g = \mathbf{i}_g = (1,0,0)^T$. Assuming that azimuth angle $\alpha_{az} = 0$, $\mathbf{n}_{axis}$ in the vehicle frame[10] can be calculated by

$$\mathbf{n}_{axis}^v = R_b^v R_g^b \mathbf{n}_{axis}^g = \begin{pmatrix} \cos\alpha_{el}\mathrm{c}_\theta\mathrm{c}_\psi + \sin\alpha_{el}\left(\mathrm{c}_\phi\mathrm{s}_\theta\mathrm{c}_\psi + \mathrm{s}_\phi\mathrm{s}_\psi\right) \\ \cos\alpha_{el}\mathrm{c}_\theta\mathrm{s}_\psi + \sin\alpha_{el}\left(\mathrm{c}_\phi\mathrm{s}_\theta\mathrm{s}_\psi - \mathrm{s}_\phi\mathrm{c}_\psi\right) \\ -\cos\alpha_{el}\mathrm{s}_\theta + \sin\alpha_{el}\mathrm{c}_\phi\mathrm{c}_\theta \end{pmatrix}. \tag{14}$$

Thus, angle ξ, which is the difference between $\mathbf{n}_{axis}^v$ and $\mathbf{n}_{ut}^v$, can be calculated as

$$\xi = \cos^{-1}\left[\left(\mathbf{n}_{axis}^v\right)^T \mathbf{n}_{ut}^v\right]. \tag{15}$$

Defining

$$\Phi_1 \triangleq \frac{\mu}{2} - \xi, \tag{16}$$

we have

$$\Sigma_1 = \int_0^{T_s} s(\tau)\,\Phi_1 \mathrm{d}\tau \tag{17}$$

$$= \int_0^{T_s} \frac{1}{2}\left(1+\mathrm{sign}\left(\xi-\frac{\mu}{2}\right)\right)\left(\frac{\mu}{2}-\xi\right)\mathrm{d}\tau \tag{18}$$

$$= \int_0^{T_s} \frac{1}{2}\left(\frac{\mu}{2}-\xi+\left\|\frac{\mu}{2}-\xi\right\|\right)\mathrm{d}\tau. \tag{19}$$

To further simplify the computation by avoiding the inverse calculation of a cosine function in Equation 15, we use the following optimization function

$$\Sigma_1' = \int_0^{T_s} \frac{1}{2}\left(\cos\xi-\cos\frac{\mu}{2}+\left\|\cos\xi-\cos\frac{\mu}{2}\right\|\right)\mathrm{d}\tau. \tag{20}$$

B. Method 2

In method 2, we minimize the relative distance between a target and the intersection of the optical axis and the ground plane, i.e., $\|\mathbf{p}_t-\mathbf{p}_l\|$ as shown in Figure 2. Given two known points $(x_1,y_1,z_1)^T$and $(x_2,y_2,z_2)^T$ in a 3D space, the equation representing the line that passes through the two points is given by the equation,

$$\frac{x-x_1}{x_2-x_1}=\frac{y-y_1}{y_2-y_1}=\frac{z-z_1}{z_2-z_1}. \tag{21}$$

When $z=0$, we have

$$x = x_1-(x_2-x_1)\frac{z_1}{z_2-z_1}, \tag{22}$$

$$y = y_1-(y_2-y_1)\frac{z_1}{z_2-z_1}. \tag{23}$$

Hence, given $\mathbf{n}^v_{axis}$, the unit vector of the optical axis in the inertial frame is $\mathbf{n}^i_{axis} \triangleq \left(n^i_{axis_n}, n^i_{axis_e}, n^i_{axis_d}\right)^T = \mathbf{n}^v_{axis}+\mathbf{p}_u$. The coordinates of the intersection between $\mathbf{n}^i_{axis}$ and the ground plane, $\mathbf{p}_l \triangleq (p_{l_n}, p_{l_e}, p_{l_d})^T$, as shown in Figure 2, can be calculated using Equations (22) and (23):

$$p_{l_n} = p_{u_n}-\frac{(n^i_{axis_n}-p_{u_n})p_{u_d}}{\left(n^i_{axis_d}-p_{u_d}\right)}, \tag{24}$$

$$p_{l_e} = p_{u_e}-\frac{(n^i_{axis_e}-p_{u_e})p_{u_d}}{\left(n^i_{axis_d}-p_{u_d}\right)}. \tag{25}$$

The new cost function for this method then becomes

$$\Phi_2 = (p_{l_n}-p_{t_n})^2+(p_{l_e}-p_{t_e})^2, \tag{26}$$

and the resulting optimization function is

$$\Sigma_2 = \int_0^{T_s} \frac{1}{2}\left(1+\mathrm{sign}\left(\xi-\frac{\mu}{2}\right)\right)\left((p_{l_n}-p_{t_n})^2+(p_{l_e}-p_{t_e})^2\right)\mathrm{d}\tau.$$

IV. Non-Gimbaled Camera Placement

The path planning of the UAV with a non-gimbaled camera for the purpose of tracking a target heavily depends on the location and the fixed camera elevation angle. In this section, we present some preliminary data showing the resulting optimal UAV trajectories based on the camera placement and suggest some criteria to consider in choosing the relative configuration of the non-gimbaled camera onboard a UAV. For this study, the target is moved with a sinusoidal motion and Method 1, described in Section III, was used to generate optimal UAV paths. We placed the non-gimbaled camera to the UAV such that the elevation angles of the camera were 30°, 60°, 90°, 120°, and 150°. Figure 3 shows both a 3D view and a top view of resulting UAV paths along with the target trajectory. It's clear that the UAV trajectories resulted from using 60° and 90° elevation angles contain relatively complex UAV maneuvers when compared to those generated with other camera configurations, while the trajectory with the camera elevation angle of 150° was the simplest. This preliminary study shows the existence of a window of optimal camera elevation angles to support desired objectives of a UAV mission.

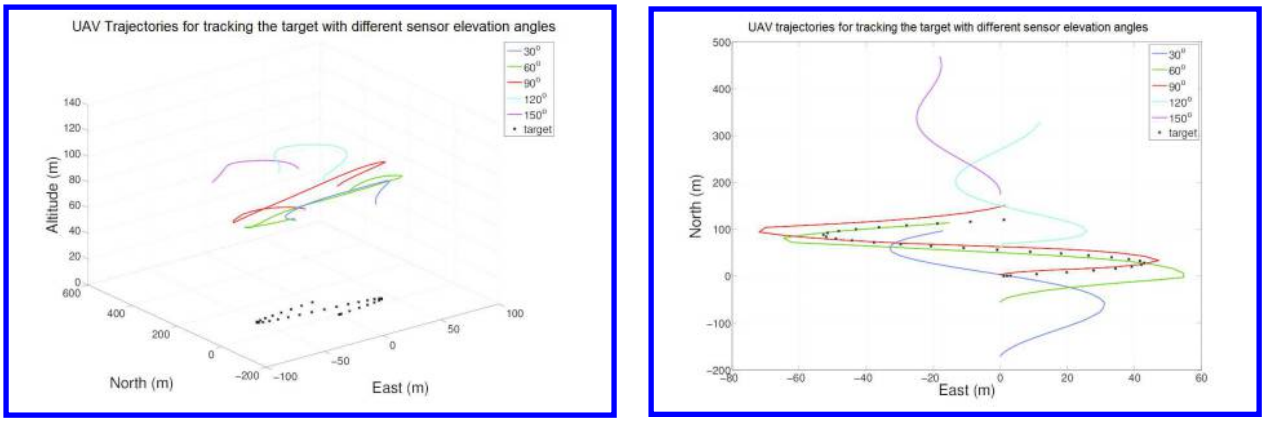

(a) 3D view. (b) Top-down view.

Figure 3. UAV trajectories generated from using different sensor placement angles.

V. Real-time Optimization Technique

We assume that the target motion is agile and unknown. To respond to the nature of the target, we use an optimization technique that incorporates a time varying look-ahead period. The "look-ahead" time horizon, T_{hor}, used in the MPC-based path planning methods, dictates the fidelity as well as the usefulness of the resulting UAV trajectories. We currently assume that target's velocity is constant during the calculation of MPC within T_{hor}. For an "agile" target, however, the larger the value of T_{hor} is, the more the difference between estimated and actual target motion results. When a target moves outside of the camera's field of view, a small T_{hor} may force a UAV to generate paths to recapture the target quickly at the cost of compromising a globally optimal UAV path that includes turn-around maneuvers. We believe finding a strategy to optimally adjust the time-varying "look-ahead" horizon based on the UAV and observed target states will be the key in finding the desired optimization solution.

Defining the distance a target traveled between time t_1 and time t_2 as

$$d(t_1, t_2) \triangleq \int_{t_1}^{t_2} \ell(\xi)\, \mathrm{d}\xi,$$

where $\ell(t)$ represents the estimated target trajectory, we can calculate accumulated distance a target traveled. Letting T_s be the time interval for current path planning, T_{hor} can be selected as

$$T_{hor}(t_k) = \begin{cases} T_{hor}(t_{k-1}) - k\left[d(t_k - T_s, t_k) - d(t_k - 2T_s, t_k - T_s)\right] & s = 1 \\ T_{hor}^{max} & s = 0, \end{cases} \tag{27}$$

where k is a positive gain and s is defined in Equation (5). Equation (27) implies that if a target is seen by the camera and the distance target traveled is increasing compared to the previous cycle, the path planning algorithm applies smaller T_{hor} to compensate the fast changing target dynamics. When the target is not observed at time t_k, a large T_{hor} should be applied to guarantee the MPC uses enough time horizon to find a feasible solution. The selections of k and T_{hor}^{max} will depend on the operational limitations of the platform and the computational capability of the onboard processor. The state transition diagram is shown in Figure 4.

VI. Estimation Strategy

To estimate the target state, a non-linear Kalman filter, called Sigma Point Kalman filter, is used when measurements are available. When the target is lost, the path optimization method described in Section III will be modified using the concept of the Sigma Point filtering, to incorporate the growth of the uncertainty and to influence UAV paths to increase the probability of recapturing the target. Techniques for estimating the target motion are typically based on Bayes's rule and Kalman Filters (KF) and its derivatives have been widely used in the past. For agile targets, Sigma-Point Kalman Filter (SPKF)[11] has shown its superior performance over estimation in the KF family.[12] Currently, techniques for estimating the state of a fast moving target uses the target dynamics model shown below:

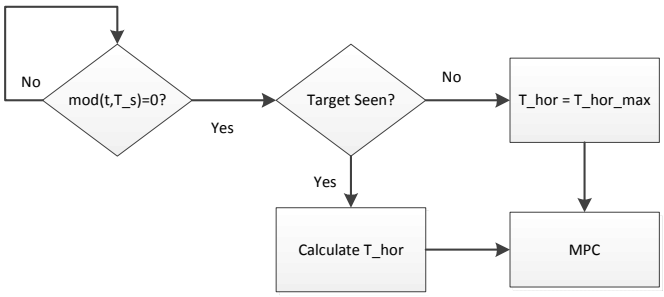

Figure 4. State transition flow chart. Function mod (a, b) returns the modulus after division of a by b.

$$\begin{aligned} \dot{p}_{t_n} &= v_t \cos\psi_t \\ \dot{p}_{t_e} &= v_t \sin\psi_t \\ \dot{v}_t &= u_1 \\ \dot{\psi}_t &= u_2, \end{aligned}$$

where p_{t_n} and p_{t_e} are the north and east coordinates of the target in the inertial frame, respectively, ψ_t is the heading angle of the target, v_t is the target velocity, and u_1 and u_2 are the control inputs to the target motion. Since inputs u_1 and u_2 are typically unknown for hostile targets, we assume that $u_1 = u_2 = 0$. For the preliminary work, we performed the target tracking task using an Extended Kalman Filter (EKF) and an SPKF, and the results are compared and presented in Figure 5. The resulting estimation errors are summarized in Table 1.

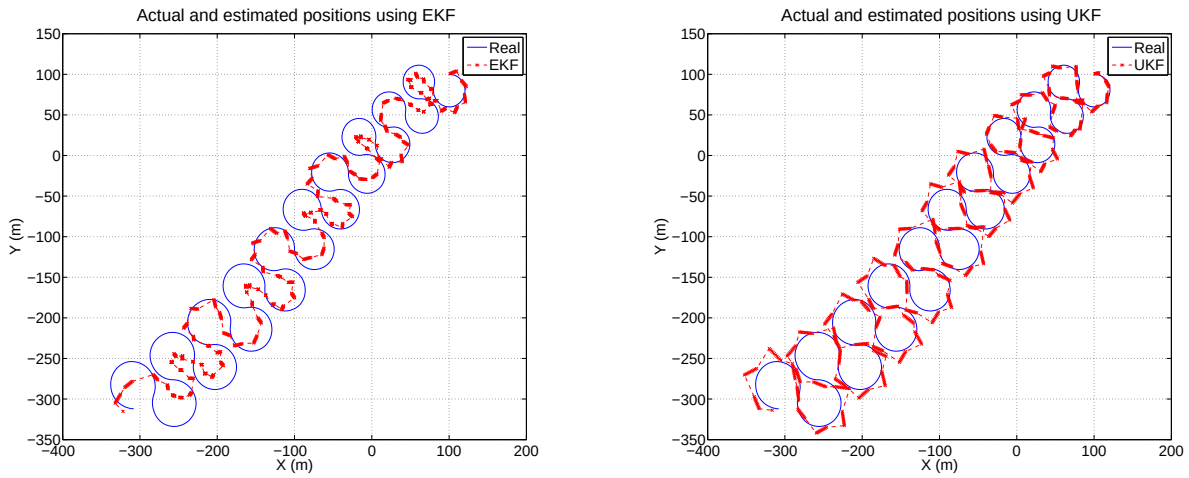

(a) EKF. (b) UKF.

Figure 5. Target position estimation results using EKF and UKF, respectively.

Table 1. Summary of Target Estimation Errors

	avg_n (m)	std_n (m)	avg_e (m)	std_e (m)	avg_{v_t} (m/s)	std_{v_t} (m/s)	avg_{ψ_t} (deg)	std_{ψ_t} (deg)
EKF	17.59	11.15	17.45	11.34	24.17	7.94	85.41	46.34
UKF	6.96	5.56	7.10	5.61	9.23	1.82	46.14	25.36
avg=average, std= standard deviation.								

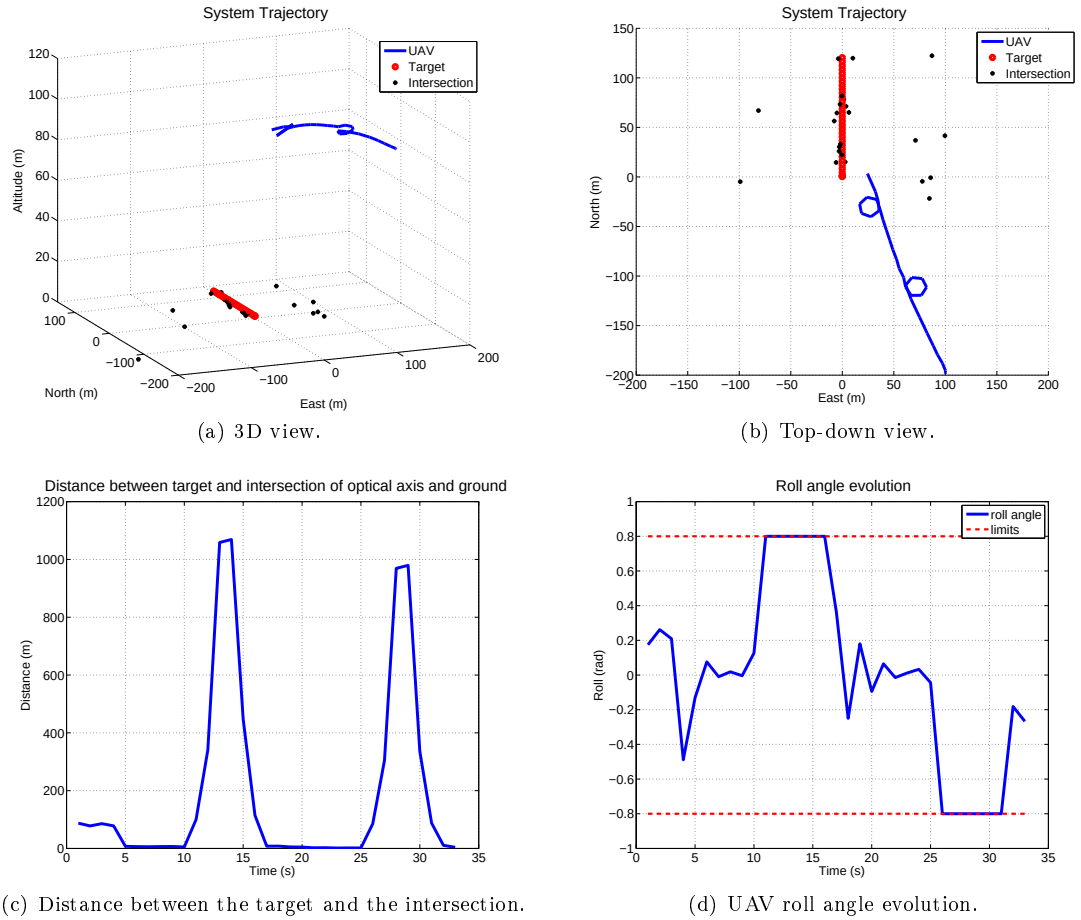

(a) 3D view.

(b) Top-down view.

(c) Distance between the target and the intersection.

(d) UAV roll angle evolution.

Figure 6. Simulation result of tracking a straight-line moving target.

VII. Simulation Results

In this section, we present the optimal path planning results generated to track a mobile target whose motion follows a straight-line and a sinusoidal trajectory, respectively.

A. Tracking a straight-line moving target

This subsection presents the results of a UAV tracking a moving target linearly using the the optimization method descried in Section III. There was no particular reason for using Method 2 instead of Method 1. The results simply show the validity of using the general optimization function in Equation 13. Figure 6 (a) shows a 3-D view of the resulting UAV path tracking a target with a constant velocity of 5 m/s heading towards the north. Figure 6 (b) shows the top-down view of the target trajectory, intersection points of the sensor axis and the ground plane, and the UAV path. Figure 6 (c) shows the distance from the target to the intersection points between the ground plane and the optical axis over the simulation period of 100 seconds. Figure 6 (d) shows the history of the roll angle of the UAV. The two circles in Figure 6 (a) and (b) represent the turn-around maneuvers of the UAV to match the relatively slow speed of the target such that the overall target observation time is maximized. The two peaks in Figure 6 (c) and the two periods in which the roll angle reaches its upper and lower limits represent the periods when the UAV was making turn-around maneuvers. The results show that the proposed path planning algorithm generates an optimal UAV trajectory.

Figure 7 shows the simulation results obtained using different time horizon periods (30 and 40 sec). It can be seen that for the same initial states of the UAV and the target motion, the resulting UAV path is heavily influenced by the selected time horizon period.

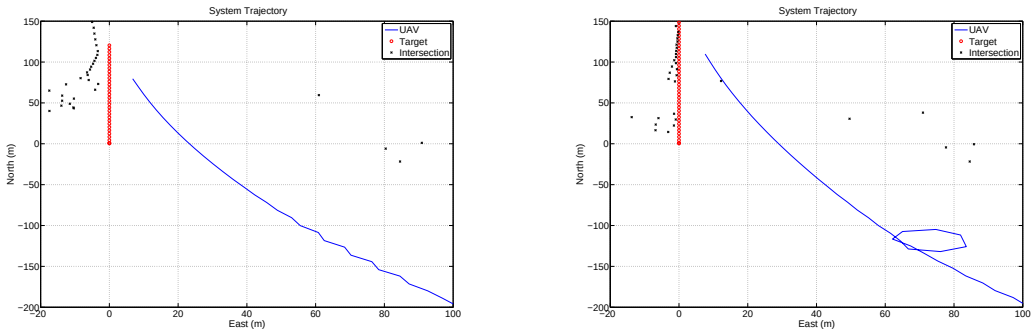

(a) 30 seconds. (b) 40 seconds.

Figure 7. UAV trajectories using different simulation times of 30 and 40 seconds, respectively.

B. Tracking a sinusoidal moving target using a time varying look-ahead horizon

Figure 8 shows the UAV trajectory resulted when a time varying T_{hor}, given by Equation (27), and the optimization function in Method 2 in Section III were used. Figure 8 (a) and (b) show the 3-dimensional and top-down views of the trajectories of the UAV (blue line) and target (red line). The black "cross" dots are the intersections of the sensor optical axis and the ground plane. Figure 8 (c) shows the time evolution of ξ, defined in Equation (15). The period $45 \sim 55$ sec in which the value of ξ is above the half of the field of view (red line) implies that the target is not seen by the sensor. Figure 8 (c) presents that the target is observed in 90% of the entire simulation time (100 s). The simulation run shows that the time-varying technique presented in Section V can be used as a basis for further investigation of finding optimal time-horizon determination, which will be based on target and UAV motion estimates.

VIII. Conclusion

In this paper, we presented novel real-time UAV path optimization algorithms to track a mobile target using a UAV with a non-gimbaled camera. Two mathematical formulations are presented to maximize the observation time of an agile ground target. Different sensor placements are used to generate the desired UAV trajectories. Simulation results are presented using both the proposed optimization functions and two nonlinear estimation techniques. Future work will focus on incorporating application specific path planning time horizon periods into the overall path planning and integration of nonlinear estimation techniques with the UAV motion.

References

[1]Dobrokhodov, V. N., Kaminer, I. I., Jones, K. D., and Ghabcheloo, R., "Vision-Based Tracking and Motion Estimation for Moving targets using Small UAVs," *Proceedings of the 2006 American Control Conference*, Minneapolis, Minnesota, USA, June 14-16 2006, pp. 1428–1433.

[2]Wang, I., Dobrokhodov, V., Kaminer, I., and Jones, K., "On Vision-Based Target Tracking and Range Estimation for Small UAVs," *AIAA Guidance, Navigation, and Control Conference and Exhibit*, No. AIAA 2005-6401, San Francisco, California, 15-18 August 2005.

[3]Hespanha, J., Yakimenko, O., Kaminer, I., and Pascoal, A., "Linear parametrically varying systems with brief instabilities: an application to vision/inertial navigation," *IEEE Transactions on Aerospace and Electronic Systems*, Vol. 40, No. 3, 2004, pp. 889–902.

[4]Geiger, B. R., Horn, J. F., Sinsley, G. L., Ross, J. A., Long, L. N., and Niessner, A. F., "Flight Testing a Real-Time Direct Collocation Path Planner," *Journal of Guidance, Control, and Dynamics*, Vol. 31, No. 6, 2008, pp. 1575–1586.

[5]Geiger, B. R., Horn, J. F., DeLullo, A. M., Long, L. N., and Niessner, A. F., "Optimal Path Planning of UAVs Using Direct Collocation with Nonlinear Programming," *AIAA Guidance, Navigation, and Control Conference and Exhibit*, No. AIAA 2006-6199, Keystone, Colorado, August 2006.

[6]Geiger, B. R., Horn, J. F., Sinsley, G. L., Long, J. A. R. L. N., and Niessner, A. F., "Flight Testing a Real Time Implementation of a UAV Path Planner Using Direct Collocation," *AIAA Guidance, Navigation and Control Conference and Exhibit*, No. AIAA 2007-6654, Hilton Head, South Carolina, 20 - 23 August 2007.

[7]Amin, J., Boškovic, J., and Mehra, R., "A Fast and Efficient Approach to Path Planning for Unmanned Vehicles," *AIAA Guidance, Navigation, and Control Conference and Exhibit*, No. 2006-6103, Keystone, Colorado, 21-24 August 2006.

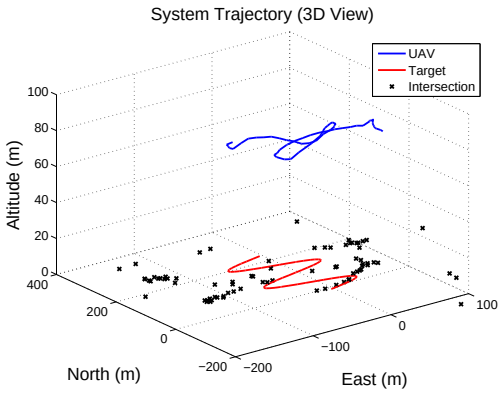

(a) 3D view.

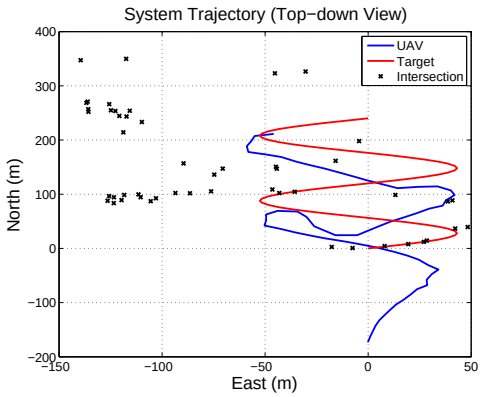

(b) Top-down view.

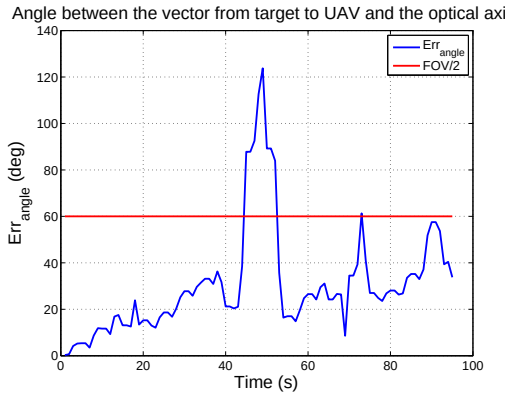

(c) Angle error.

Figure 8. Simulation result using a time varying horizon in tracking a sinusoidal moving target.

[8]Toupet, O. and Mettler, B., "Design and Flight Test Evaluation of Guidance System for Autonomous Rotorcraft," *AIAA Guidance, Navigation, and Control Conference and Exhibit*, No. 2006-6201, Keystone, Colorado, 21-24 August 2006.

[9]Rysdyk, R., "Unmanned Aerial Vehicle Path Following for Target Observation in Wind," *AIAA Journal of Guidance, Control, and Dynamics*, Vol. 29, No. 5, 2006, pp. 1092–1110.

[10]Beard, R. W. and McLain, T. W., *Small Unmanned Aircraft: Theory and Practice*, Princeton University Press, 2012.

[11]Thrun, S., Burgard, W., and Fox, D., *Probabilistic Robotics*, The MIT Press, 2005.

[12]Plett, G. L., de Lima, P., and Pack, D. J., "Target Localization using Multiple UAVs with Heterogeneous Sensors," *AIAA Infotech@Aerospace Conference and Exhibit*, No. AIAA-2007-2845, Rohnert Park, California, May 7-10 2007.